Ideal metastability fields and field penetration in type-I and type-II superconducting *In*Bi single spheres

Guy Pettersen* and Hugo Parr†
Institute of Physics, University of Oslo, Blindern, Oslo 3, Norway
(Received 24 August 1978)

In a continuation of earlier work on the *In*Bi alloy system, we have studied the superconductive properties of small, single spheres of *In*Bi 0.80-, 1.24-, 1.70-, 2.15-, and 2.65- at.% Bi. The transition temperatures are 3.538, 3.659, 3.796, 3.908, and 4.044 ± 0.008 K. Assuming the penetration depth λ to be proportional to $y = 1/(1-t^4)^{1/2}$, we determine $\lambda_0 = d\lambda/dy$ to be 810, 950, 1065, undetermined, and 1720 Å ± 3%, respectively. The field dependence of λ was studied up to the ideal superheating field H_{sh}. We find $\lambda(H_{sh})/\lambda(H=0) = 1.53$, 1.52, 1.42, undetermined, and 1.41 ± 0.05, respectively. Thus the relative increase in λ close to H_{sh} is roughly independent of composition. These are the first measurements of $\lambda(H)$ in "strong" fields for type-II superconductors. The Ginzburg-Landau parameter κ was determined from H_{c3}. We find $\kappa_{c3}(t=1) = 0.454$, 0.636, 0.835, 0.984, and 1.22. The knowledge of H_c limits the accuracy to 2–5%. Ideal superheating was observed both in the type-I and type-II region. At $t=1$, we find $H_{sh}/H_c = 1.80$, 1.48, 1.28, 1.17, and 1.13 ± 3–8%. This roughly agrees with numerical calculations of $H_{sh}(\kappa)$. Thus, ideal superheating of the Meissner state to well above H_c is firmly established even for type-II superconductors. The results for H_{sh} are in good agreement with numerical calculations from Ginzburg-Landau theory. Assuming these theoretical results to hold, $\kappa(t=1)$ can be calculated self-consistently from H_{c3} and H_{sh} for all metals investigated by the single-sphere method, giving values considered to be more accurate than any others available. Finally, we have obtained qualitative and quantitative results on the intermediate and mixed states in our spheres.

I. INTRODUCTION

Hysteresis, and the ideal metastability limits of the different critical fields occurring in superconductors, are most easily studied in small, single spheres.[1–6] Spheres with diameters in the range 10–30 μm exhibit essentially bulk behavior, yet they can be produced without the flaws and defects that lead to heterogeneous nucleation in macroscopic samples, thus preventing the observation of ideal superheating and supercooling. The present work completes a systematic investigation of these properties as a function of the Ginzburg-Landau parameter κ. The main objectives are to study the ideal superheating field H_{sh}, and the field dependence of the penetration depth λ in "strong" fields approaching H_{sh}. The *In*Bi alloy system was chosen because it is convenient to work with, and because a good deal was known about its superconductive properties.[7,8] In previous work,[5,6] we investigated the composition range of 0–0.6-at.% Bi, with κ ranging from 0.061 in pure In to 0.349. We now present results for compositions ranging from 0.8 to 2.65-at.% Bi, corresponding to κ values of 0.45 – 1.22. We are especially interested in the crossover from type-I to type-II superconductivity which occurs in the middle of this composition range.

II. THEORY

The groundwork for the analysis and interpretation has been laid in our previous work on Sn,[4] and *In*Bi.[5,6] In the following, we briefly recall some of the main points. For a full reasoning and justification, the earlier papers must be consulted.

A. Penetration depth

The information about the penetration depth is carried in the magnitude of the signal jump $S(T,H)$ from the Meissner state to the normal state. Thus S decreases as we have $T \to T_c$, and as we have $H \to H_{sh}$. (See for instance Fig. 1 of Ref. 4.) We assume a penetration depth $\lambda(T,H) = \lambda_0 y f(H/H_{sh})$, with $y = 1(1-t^4)^{1/2}$. For $H=0$, the temperature dependence of the signal is then given by

$$S(T,0) = \frac{S(0,0)[1 - 3\lambda_0 y/R + 3(\lambda_0 y/R)^2]}{1 - 3\lambda_0/R + 3(\lambda_0/R)^2} , \quad (1)$$

where R is the sphere radius. Fitting the experimental data to Eq. (1), λ_0 and $S(0,0)$ are obtained. In order to analyze the field dependence of λ, the tem-

perature dependence of λ is normalized away by defining a reduced signal

$$\zeta(h) = [S(T,h) - S^0]/[S(T,0) - S^0] \ . \quad (2)$$

Here S^0 is the signal extrapolated to zero penetration depth, i.e., Eq. (1) with $y = 0$, and h is the reduced equatorial field

$$h \equiv H_{eq}/H_{sh} \cong k(T) H/H_{sh} \ , \quad (3)$$

$$k(T) = \tfrac{3}{2}[1 - \lambda_0 y/R + (\lambda_0 y/R)^2] \ ,$$

where H is the applied field. In the spherical geometry, the field at the surface varies from 0 at the pole to H_{eq} at the equator, given by Eq. (3). Note that the demagnetization coefficient of Eq. (3) is temperature dependent and somewhat less than the bulk value of $\frac{3}{2}$, typically 2 − 10%. The decrease in signal with increasing H is related to an "averaged" penetration $\bar{\lambda}$ given by

$$\frac{\bar{\lambda}(h)}{\lambda(0)} \equiv \bar{f}(h) = \int_0^{\pi/2} d\theta \sin\theta f(h \sin\theta) \ , \quad (4)$$

where the integration is over polar angle, i.e., from the pole to the equator of the sphere. We have shown that, to first order in λ/R, the reduced signal is related to $\bar{f}(h)$ by

$$\zeta_\perp(h) \cong \bar{f}(h) \ , \quad (5)$$

(tickling field perpendicular to static field) and

$$\zeta_\parallel(h) \cong \frac{d}{dh}[h\bar{f}(h)] \ . \quad (6)$$

(tickling field parallel to the static field). Because $\lambda(h)$ increases very strongly close to the superheating limit at $h = 1$, the field effect is much easier to measure in parallel fields. As seen from Eq. (6), the reduced signal $\zeta_\parallel$ must then be integrated over field h to obtain the averaged penetration depth $\bar{\lambda}(h)$, then Eq. (4) must be inverted empirically to obtain the real field dependence $\lambda(h)$.

There is no general, analytic prediction for $\lambda(h)$ for general values of κ. However, in the limit $\kappa \to 0$, the field dependence is just the inverse of the reduced surface order parameter ψ_s/ψ_0, which was computed by the authors of Ref. 9, i.e.,

$$\lambda(H)/\lambda(0) = [\psi_s(H)/\psi(0)]^{-1} \ , \quad (7)$$

$$\psi_s(H)/\psi(0) = 2^{-1/2}\{1 + [1 - (H/H_{sh})^2]^{1/2}\}^{1/2} \ . \quad (8)$$

At H_{sh}, this gives $\psi_s/\psi_0 = 1/2^{1/2}$ and $\lambda(H_{sh}) = 2^{1/2}\lambda(H = 0)$. For finite κ, the surface order parameter is further decreased compared to Eq. (8). However, Eq. (7) no longer holds, so the effect on $\lambda(H)$ cannot be immediately ascertained. In fact, there are two conflicting predictions: a proof by Esfandiari and Fink[10] that we have $\lambda(H_{sh}) = 2^{1/2}\lambda(0)$ for all κ, and an analytic calculation by one of us,[11] giving to first order in κ,

$$\lambda(H_{sh})/\lambda(0) = 2^{1/2}[1 + 3(2)^{1/2}\kappa/32] \ . \quad (9)$$

Previous experiments did not resolve this conflict, because κ was too low to give significantly different predictions. The present experiments should be more suited, since κ now goes well beyond 1. In general we will still compare our detailed results to Eqs. (7) and (8), since no other analytical expression is available. As the results will show, the low-κ calculation describes the results surprisingly well even in the type-II domain. It would be useful if a detailed analytical or numerical calculation of $\lambda(H)$ was made for different values of κ, for instance $\kappa = 0.1$, 0.4, 0.7, 1.0, 1.5 and 5.

B. Transition fields

Apart from the thermodynamic critical-field $H_c(T)$, we shall be concerned with the following fields:

$$H_{c2} = \kappa(2)^{1/2} H_c \ , \quad (10)$$

$$H_{c3} = 1.695 H_{c2} = 2.397 \kappa H_c \ , \quad (11)$$

$$H_{sh} \cong [\kappa(2)^{1/2}]^{-1/2}[1 + 15(2)^{1/2}\kappa/32] H_c \quad (\kappa \ll 1) \ , \quad (12)$$

$$H_{sh} \cong (5^{1/2}/3)[1 + (2\kappa)^{-1/2}] H_c \quad (\kappa \gg 1) \ , \quad (13)$$

$$H_{c1} \cong (H_c \ln\kappa)/(2^{1/2}\kappa) \quad (\kappa \gg 1) \ , \quad (14)$$

$$H_D \cong H_c/k(T) \quad \text{for } \kappa < 1/2^{1/2} \ . \quad (15)$$

These equations are valid for bulk, local superconductors. In the type-II domain, H_{c2} and H_{c3} mark the onset of the bulk mixed state and of surface superconductivity respectively, by second-order phase transitions. In low-κ materials, H_{c2} and H_{c3} are the fields at which homogeneous nucleation of bulk or surface superconductivity takes place irreversibly. H_{sh} is the superheating field of the Meissner state both in the type-I and type-II domain. Equation (12) is the instability field obtained from one-dimensional Ginzburg-Landau (GL) theory.[9,11] H_{sh} is correct to second order in κ for small κ, and is good to 4% at $\kappa = 0.5$ and 10% at $\kappa = 1$. Numerical calculations are also available.[12–14] Equation (13) is the three-dimensional instability field which becomes lower than the one-dimensional field for $\kappa \gtrsim 1.1$.[13] It is good to 1%. H_{c1} is the equilibrium transition field from the Meissner state to the mixed state. H_D is the demagnetization field for a sphere, with $k(T) \lesssim \frac{3}{2}$ given by Eq. (3). This field marks the thermodynamic equilibrium between the Meissner state and the intermediate state in a sample with

nonzero demagnetization factor. Its study is interesting in its own right, since it exhibits a large size effect governed by the length Δ characterizing the surface energy of a normal-to-superconducting wall.

Figure 1 sums up the different fields, normalized to H_c, as a function of κ. Note that for a sphere, the transitions at H_{sh} and H_{c1} will occur when the *equatorial* field H_{eq} reaches the critical value. The observed, applied field H must therefore be multiplied by the factor $k(T)$ in Eq. (3), before comparison with theory. No such factor occurs for H_{c3} or H_{c2}.

III. EXPERIMENTAL TECHNIQUE AND SAMPLES

The cryostat and detection system have been described before.[3–6] We use lock-in detection at 75 kHz, with a peak-to-peak tickling field of 0.4–0.5 Gauss. The effects of the tickling field are corrected for. The static field can be parallel or perpendicular to the tickling field. Temperature can be stabilized to 0.2 mK.

The spheres are produced by ultrasonic dispersion of the molten metal in glycerol.[6] The alloys were prepared by the Central Institute of Industrial Research in Oslo. The concentration was determined by x-ray fluorescence spectrometry. We present here our measurements of the bulk resistivity of the series of alloys prepared.

Four-point resistance measurements were made at 293, 80 and 4.2 K on wires made by extrusion. The wires were 80 mm long and 1 mm in diameter. Absolute resistivities were determined to 10% accuracy, while resistance ratios are accurate to better than 3%. For each alloy, the mean-free-path l at 4.2 K was computed using the relation $\rho_{bulk}\, l = 5.4 \times 10^{-12}$ Ω cm^2, derived from size effect measurements.[15] Table I gives the results. Figure 2 shows ρ at 4.2 K and the residual resistance ratio RRR as a function of Bi content. The recent results of Yogi are also included.[16] The two sets of data are in excellent agreement, and together give a closely linear increase in ρ(4.2 K) with Bi content. The slope is 1.71 $\mu\Omega$ cm/at.% Bi.

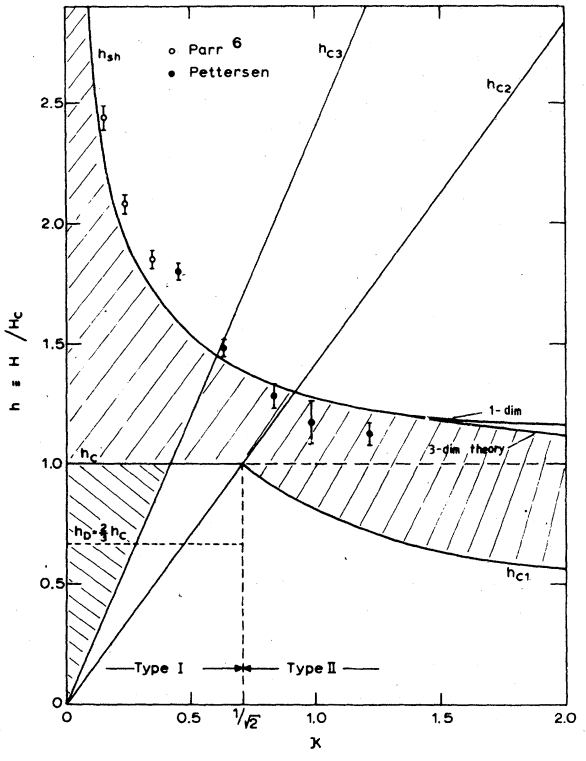

FIG. 1. Overview of the different transition fields occurring in type-I and type-II superconductors, normalized to H_c. Hatched areas indicate the possible superheating of the Meissner state (up to h_{sh}) or supercooling of the normal state (down to h_{c3} for κ below 0.417). H_{sh} is given by one-dimensional GL theory up to $\kappa \approx 1.1$, and by three-dimensional GL theory above 1.1. Also shown are our experimental values for h_{sh} in the *In*Bi alloy series (Sec. IV). h_D is the reduced demagnetizing field for a sphere.

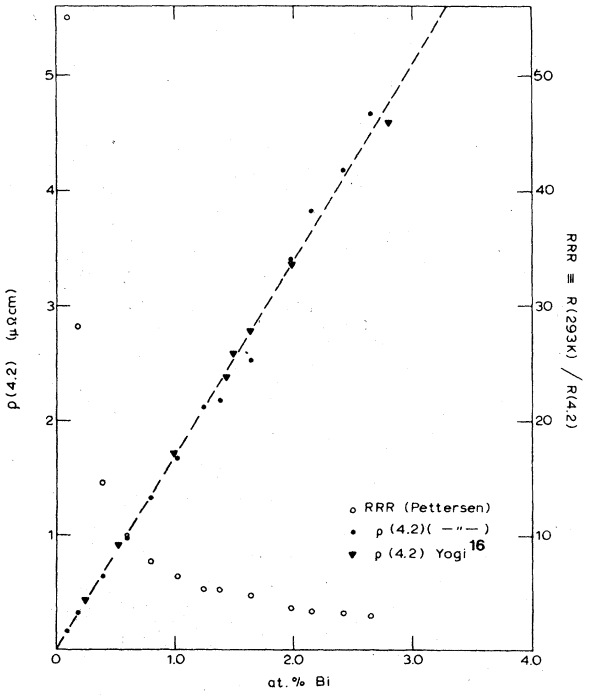

FIG. 2. Resistivity at 4.2 K and Residual Resistance Ratio for the *In*Bi alloys. Uncertainties are about 10% in ρ, and 3% in RRR. Straight line is least squares fit of all data points shown. Slope is 1.71 $\mu\Omega$ cm per at.%.

TABLE I. Bulk resistivity of the *In*Bi alloys.

Bi concentration (at.%)	ρ(298 K) ($\mu\Omega$ cm)	ρ(80 K) ($\mu\Omega$ cm)	ρ(4.2 K) ($\mu\Omega$ cm)	RRR $=\frac{\rho(293\text{ K})}{\rho(4.2\text{ K})}$	l(4.2 K) (μm)
0.0	8.69	1.74	(~0.0005)	(>16 000)	>300
0.104	8.77	1.84	0.16	55.0	0.875
0.19	8.99	2.01	0.32	28.2	0.438
0.395	9.27	2.37	0.64	14.6	0.220
0.60	9.72	2.73	0.97	10.0	0.144
0.80	10.22	3.11	1.33	7.69	0.105
1.02	10.65	3.48	1.67	6.35	0.0837
1.24	11.11	3.96	2.12	5.24	0.0660
1.40	11.39	4.27	2.18	5.22	0.0642
1.70	11.91	4.68	2.53	4.71	0.0552
1.98	12.48	5.30	3.41	3.66	0.0409
2.15	12.94	5.66	3.83	3.38	0.0365
2.42	13.29	6.07	4.19	3.17	0.0334
2.65	13.86	6.60	4.67	2.97	0.0300
4.90	17.19	9.83	6.37[a]	2.70	0.0220

[a]This alloy had T_c slightly above 4.2 K. The resistivity given is that measured just before the superconductive transition.

IV. RESULTS AND DISCUSSION

A. Critical temperature and $H_c(T)$

Transition temperatures were determined for each sphere by averaging 4–6 zero-field temperature sweeps.[3,6] For any one sphere in a particular cooldown, T_c is thus determined to ± 0.2 mK, and the temperatures sweeps are reversible to this accuracy. A small, remanent axial field of 0.2 G was corrected for. Different spheres of the same composition give T_c's differing by 1–8 mK. On an absolute scale, the calibration of our Ge thermometer is good to 5 mK.[6]

Table II gives the results, including the previous *In*Bi measurements below 0.6 at.%.[6] Figure 3 shows T_c versus composition. The initial decrease in T_c is due to the smearing-out of the energy gap anisotropy, similar to what was observed on *In*Pb. Above 0.4-at.% Bi, T_c increases linearly with composition, with a slope 0.27 K / at.%.

The choice of $H_c(T)$ is critical for the interpretation of the superheating and supercooling results. For pure In, $H_0 = 281.53 \pm 0.06$ Gauss,[17] and the deviation from a parabola is well approximated by

$$D(t^2) = H_c(T)/H_0 - (1 - t^2) \cong -0.021 \sin(\pi t^2) \quad . \quad (16)$$

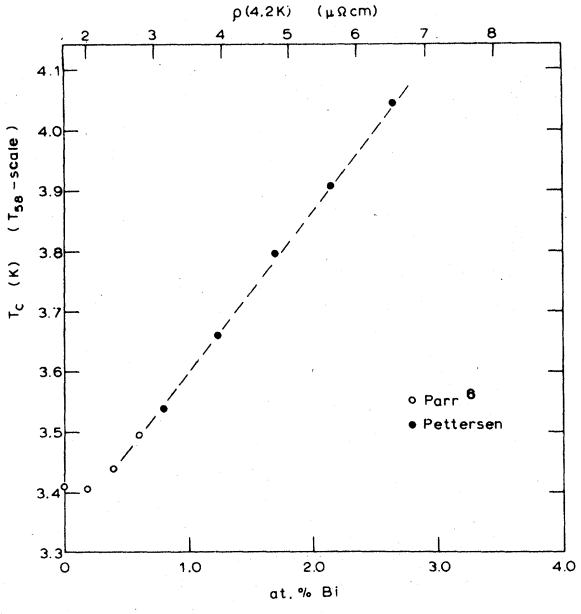

FIG. 3. Transition temperatures for the *In*Bi alloys. Initial dip below 0.2 at.% is due to the smearing out of the energy gap anisotropy by the added impurities. Straight line has the equation $T_c = 3.33 + 0.27x$ K, where x is the concentration in at.%.

TABLE II. Experimental parameters of *In*Bi spheres.

Bi conc. (at.%)	0.0	0.19	0.39	0.60	0.80	1.24	1.70	2.15	2.65
$2R$ (μm)	18.6	18.1	18.8	17.8	19.0	18.9	15.7	16.8	20.2
λ_0 (Å)	395 ±15	500 ±20	630 ±20	675 ±20	810 ±30	950 ±35	1065 ±50	(1375) (calc.)	1720 ±50
T_c (K) (^{4}He scale)	3.409	3.405	3.440	3.495	3.538	3.659	3.796	3.908	4.044
H_0 (G)	278 calc.	278 calc.	280 calc.	284 meas.	285 meas.	315 meas.	350 calc.	385 calc.	405 calc.

With increasing Bi content, H_0 increases, and, presumably, the deviation from a parabola is slowly reduced. However, this change is very slow,[18] and there are no such detailed data available for *In*Bi. Therefore, we chose to fit existing data to Eq. (16), with H_0 as the only parameter. Our previous measurements of H_c in 0.6 at.% gave $H_0 = 284 \pm 3$ G.[6] We made similar measurements in the 0.8- and 1.24-at.% spheres, although the interpretation of H_c is somewhat less clear cut. This gives $H_0 = 285$ and 315 ± 6 G, respectively. In the type-II domain, we cannot measure H_c. We therefore use the magnetization measurements of Kinsel *et al.*[7] Figure 4 shows the different measurements of H_0 in *In*Bi. Assuming Eq. (16) for $D(t^2)$, the slope of H_c at T_c is given by

$$\left(\frac{dH_c}{dT}\right)_{T_c} = \frac{-1.87 H_0}{T_c} \quad . \tag{17}$$

Kinsel *et al.* measured both this slope and H_0. As the figure shows, the values of H_0 derived from the slope are the most consistent. The full curve is our empirical, final choice for H_0. It gives $H_0 = 350$, 385, and 405 G, for *In*Bi 1.70, 2.15, and 2.65 at.% respectively. We have no physical explanation for the "kink" around 1 at.%. This may indeed by the point where $D(t^2)$ starts to change appreciably.

In conclusion, we believe our measured and calculated values of $H_c(T)$ near T_c (above $t = 0.8$) to be good to 2–3% in the type-I domain and 4–5% in the type-II domain. As we shall see, this will dominate the uncertainty in determining the GL parameter and interpreting the superheating results.

B. Temperature and field dependence of the penetration depth

The signal difference $S(T,H)$ between the Meissner state and the normal state can be determined to 1–2% accuracy.[4,5] The signal time drift must be corrected for.[4,5] For $H = 0$, we then fit the results to Eq. 1, obtaining $S(0,0)$ and λ_0. Figure 5 shows the normalized results, as a function of $y = (1 - t^4)^{-1/2}$. Solid curves show best fits for λ_0. The fits are very good all the way up to $y = 11 (t \approx 0.998)$. This verifies that T_c has been correctly determined, and that

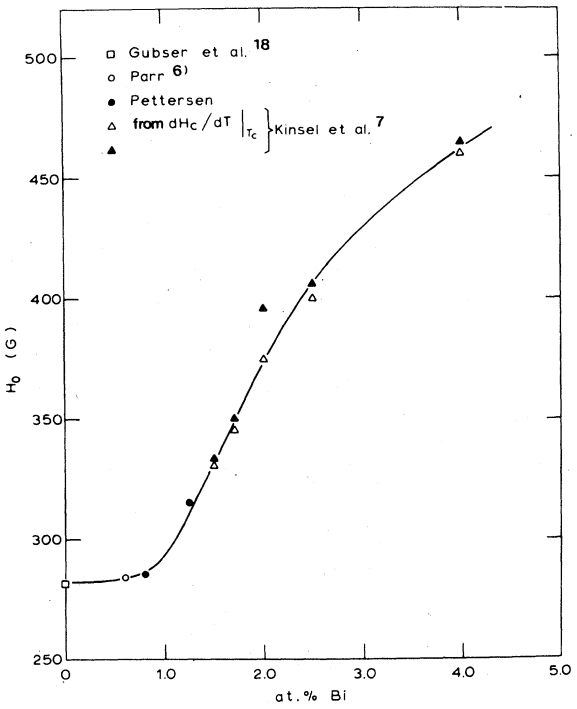

FIG. 4. Thermodynamic critical field H_0 at $t = 0$. Our values have been found by extrapolation, assuming the deviation function $D(t^2)$ given in the text. H_0 from $dH_c/dT|_{T_c}$ has been calculated from Eq. (17). Solid line is drawn by hand.

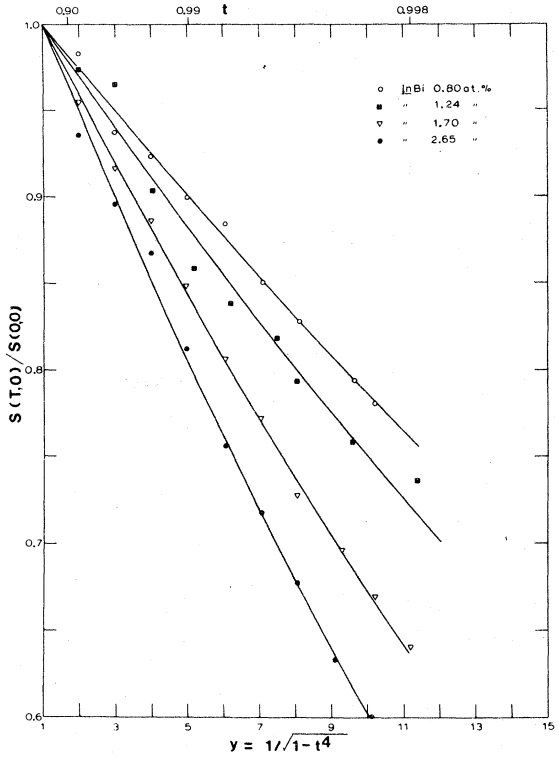

FIG. 5. Temperature dependence of transition signal $S(T)$, due to the increase in penetration depth with temperature. Solid curves are fits to Eq. (1), giving $S(0,0)$ and λ_0.

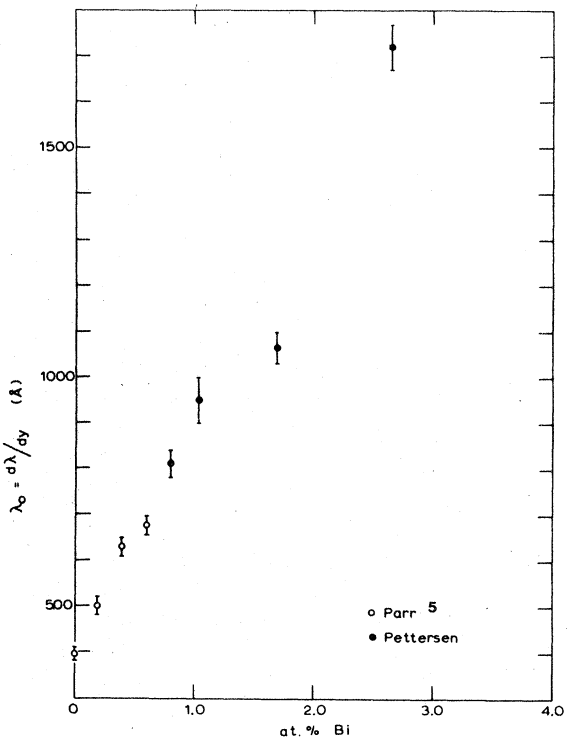

FIG. 6. Penetration depth $\lambda_0 = (= d\lambda/dy)$ as a function of Bi concentration. There seems to be no saturation in the increase of λ with impurity content.

the assumption $\lambda \cong \lambda_0 y$ is valid above $y = 2$. The values of λ_0 and sphere diameter R are given in Table II. Figure 6 shows λ_0 as a function of composition. From a value of 395 Å in pure In, λ_0 increases almost linearly to 1720 Å in *In*Bi 2.65 at.%. There seems to be no saturation in the increase of λ_0. Unfortunately, $\lambda(T,H)$ could not be determined for the 2.15-at.% sphere, so this conclusion is somewhat uncertain.

The field dependence $S(H)$ was obtained by doing sweeps at constant temperature close to T_c, and graphically measuring $S(H)$ from the recorder trace.

TABLE III. Field dependence of the penetration depth. Note: Parameters are best fit to $\lambda(H)/\lambda(0) = [\psi_s(H)/\psi_s(0)]^{-1} + Ah^2 + Bh^4 + Ch^6$.

at.% Bi	0.80 ($y \simeq 4$)	0.80 ($y \simeq 5$)	1.24	1.70	2.65 ($y \simeq 3$)	2.65 ($y \simeq 5$)
$\kappa(t=1)$	0.454	0.454	0.636	0.835	1.218	1.218
$\bar{\lambda}(H_{sh})/\lambda(0)$	1.25	1.25	1.21	1.18	1.18	1.18
$\lambda(H_{sh})/\lambda(0)$	1.52	1.54	1.52	1.42	1.42	1.40
$\alpha \equiv \frac{d\lambda}{dh^2}\|_0$	0.63	0.33	0.01	0.14	0.13	0.17
A	0.509	0.201	−0.114	0.014	0.002	0.047
B	−0.945	−0.233	0.196	0.009	0.085	0.107
C	0.539	0.156	0.026	−0.020	−0.078	−0.170

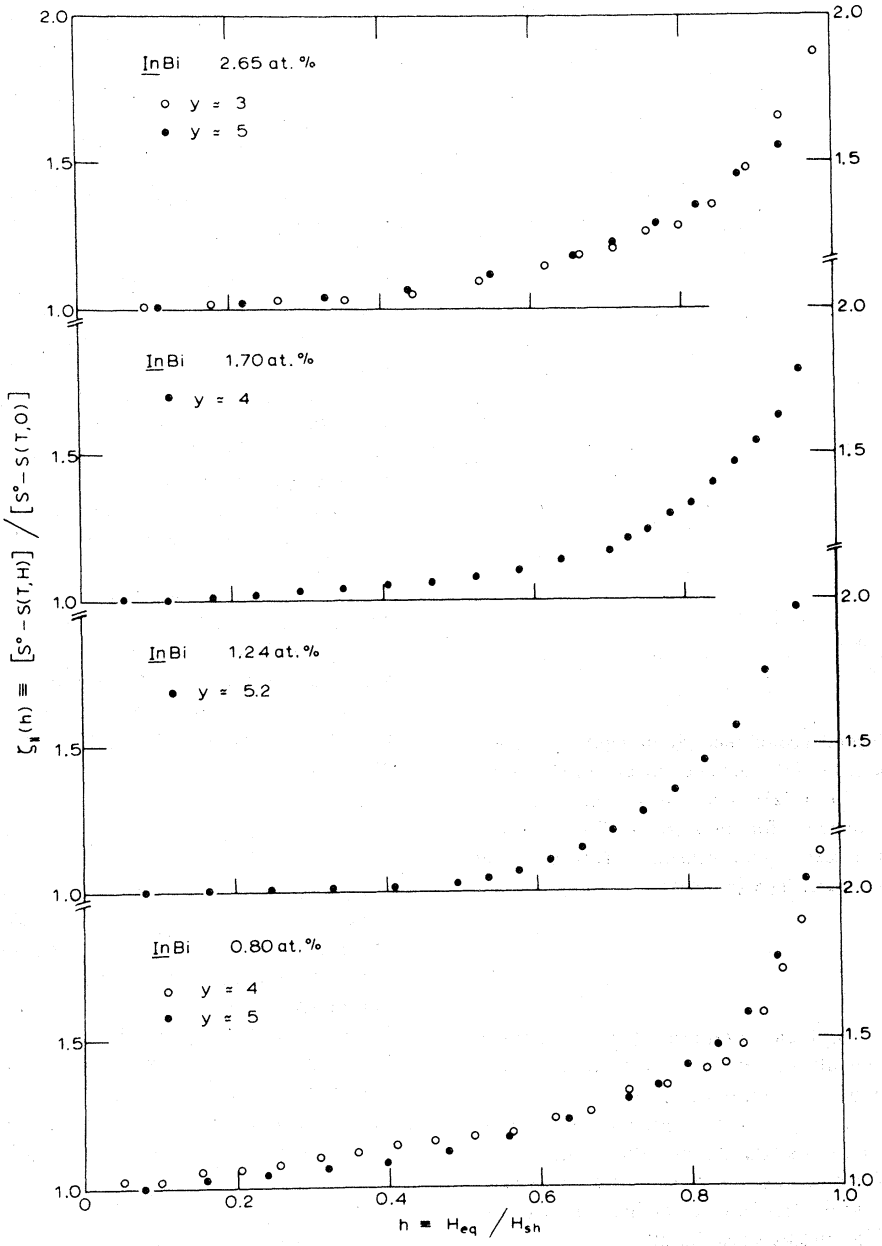

FIG. 7. Field dependence of transition signal S, given as reduced signal $\zeta_{\parallel}(h)$. Note strong increase close to the superheating field H_{sh}. $(h=1)$.

(See for instance Fig. 1 of Ref. 4.) In order to obtain maximum sensitivity, yet avoid the size effect region,[6] we chose $0.97 < t < 0.99$, i.e., $3 < y < 5$. The measurements were done with the static field parallel to the tickling field. Figure 7 shows the results for the reduced signal $\zeta_{\parallel}(h)$ [Eq. (2)]. The main uncertainty here comes from the correction for signal time drift,[5] which was assumed to be linear in time during the 1–5 minutes needed to make the field sweep. If the drift is not linear, systematic errors in $\zeta_{\perp}$ can result. Such errors could cause the differences seen at low $h\,(h < 0.6)$ in the figure. Close to $H_{sh}(h=1)$, the field effect gets bigger, and any such error becomes less serious.

The next step is integration over h [Eq. (6)] to obtain the averaged field dependence $\bar{f}(h) = \bar{\lambda}(h)/\lambda(h=0)$. Figure 8 shows $\bar{f}(h)$ for the "dirtiest" alloy studied, compared to the low-κ GL prediction, Eqs. (7) and (8). Figure 9 shows the final results for the field-dependent penetration depth

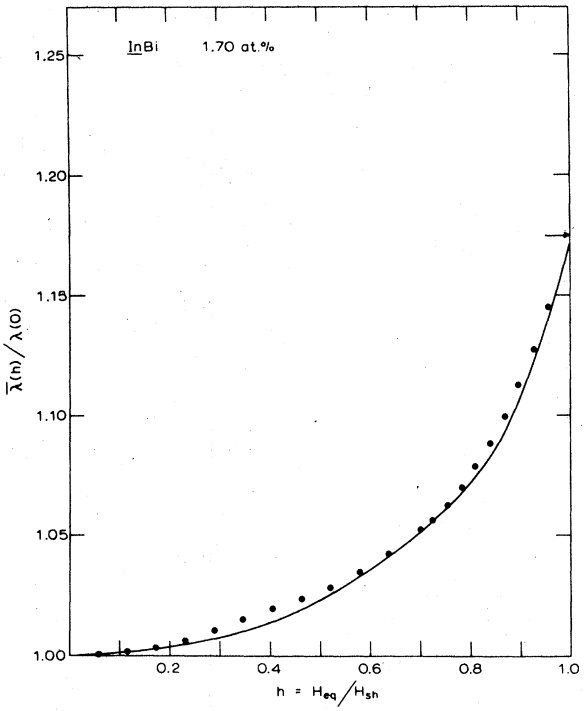

FIG. 8. Field dependence of penetration depth $\bar{\lambda}$ averaged over sphere surface, Eq. (4). Obtained by graphical integration of data in Fig. 7 [Eq. (2)]. Only one concentration is shown. The GL prediction for low κ [Eq. (7)] is given by the solid line. Fit is seen to be excellent. This is somewhat surprising since κ is quite high (=0.835).

$\lambda(H/H_{sh})$, after empirical inversion of the data for $\bar{f}$.[5] Table III gives all the inversion parameters, and the main results of the field dependence.

The value of λ at H_{sh} is of particular interest. On the one hand, there is a prediction[10] that it should equal $2^{1/2}\lambda(0)$ for all κ, on the other hand there is the calculation[11] giving its first-order increase with κ [see Eq. (9)]. The present results give $\lambda(H_{sh})/\lambda(H=0)=1.53$, 1.52, 1.42, and 1.41 ± 0.05 for *In*Bi 0.80, 1.24, 1.70, and 2.65 at.%, respectively. The corresponding κ values are 0.45, 0.64, 0.84, and 1.22 (Sec. IVC). In Fig. 10, we have plotted all available data for $\lambda(H_{sh})/\lambda(0)$ in Sn,[4] and past[5] and present *In*Bi measurements. The measurements seem to be consistent with the constant value of $2^{1/2}\cong 1.41$. In contrast, Eq. (9) predicts 1.64 for the highest value of κ studied, seemingly outside of the experimental uncertainty. [A note of caution: as κ increases, H_{sh}/H_c decreases, so the tickling field increases relative to H_{sh}. This means that measurements of $\lambda(H)$ cannot be carried out quite so close to H_{sh}.]

We have checked the mathematics leading to Eq. (9). The salient point is the calculation of the surface order parameter f_0, see Eq. (13) of Ref. 11, giving

$$f_0(H_{sh}) \cong (1/2^{1/2})[1-7(2)^{1/2}\kappa/32] \ .$$

If the number 7 was changed to 4, terms would cancel out so that $\lambda(H_{sh})/\lambda(0)$ would equal $2^{1/2}$, independent of κ to first order in κ. However, we have found no mistakes. Let us point out also that any such change in f_0 would *not* change the main result of Ref. 11, namely, the calculation of H_{sh}, [Eq. (12)] because the mathematics are such that only the 0th order term $f_0-1/2^{1/2}$ is involved in that result.

In conclusion, we have measured $\lambda(H)$ in strong fields approaching the bulk superheating field H_{sh} for κ values ranging from 0.45 to 1.22. It is the first time such measurements have been carried out in type-II superconductors. Figure 9 shows that the field dependence comes quite close to being independent of κ, when expressed in reduced coordinates. There may be real deviations at low field, i.e., $H/H_{sh} \ll 1$, yet we have seen that they may reflect systematic errors. The GL prediction for low κ, Eqs. (7) and (8), fits the data rather well. Surprisingly, it is most accurate for the higher κ values. ($\kappa=0.84$ and 1.22).

C. H_{c2}, H_{c3}, and the Ginzburg-Landau parameter

H_{c3} is readily identified in all our samples as the highest field at which the signal differs from the normal state. H_{c2} could only be identified in the type-II samples. H_{c3} could be seen in both parallel and perpendicular fields, H_{c2} only in parallel fields. Figure 11 shows $\kappa_{c3}(t)$, obtained from Eq. (11). $\kappa_{c3}(t=1)$ is obtained by linear extrapolation to $t=1$. κ_{c2} is similarly obtained from Eq. (10). Yet another estimate of κ may be obtained from the resistivity by assuming the Gorkov-Goodman relation[19]

$$\kappa = \kappa_0 + 7.5\times 10^3 \gamma^{1/2}\rho \ , \qquad (18)$$

where we have $\kappa_0=0.061$,[6] and $\gamma=1088$ erg/cm^{3}K^2 for pure In,[18] and ρ is measured in Ω cm. Table IV gives the different values of κ and their temperature derivatives. We consider $\kappa_{c3}(t=1)$ the most reliable estimate of the GL parameter. The main uncertainty involved is that of $H_c(t)$, discussed earlier. The values for κ_{c2} are seen to be 3–5% higher. To check the predictions of the Gorkov-Goodman (GG) relations, we have plotted in Fig. 12 $\Delta\kappa=\kappa_{meas.}-\kappa_{GG}$, as a function of composition. Up to 0.8 at.%, the slope of κ_{c3} versus composition is about 15% higher than the slope predicted by Eq. (18). Then the difference starts diminishing and vanishes around 2 at.%, within the experimental accuracy. This corresponds to $\kappa\approx 0.9$.

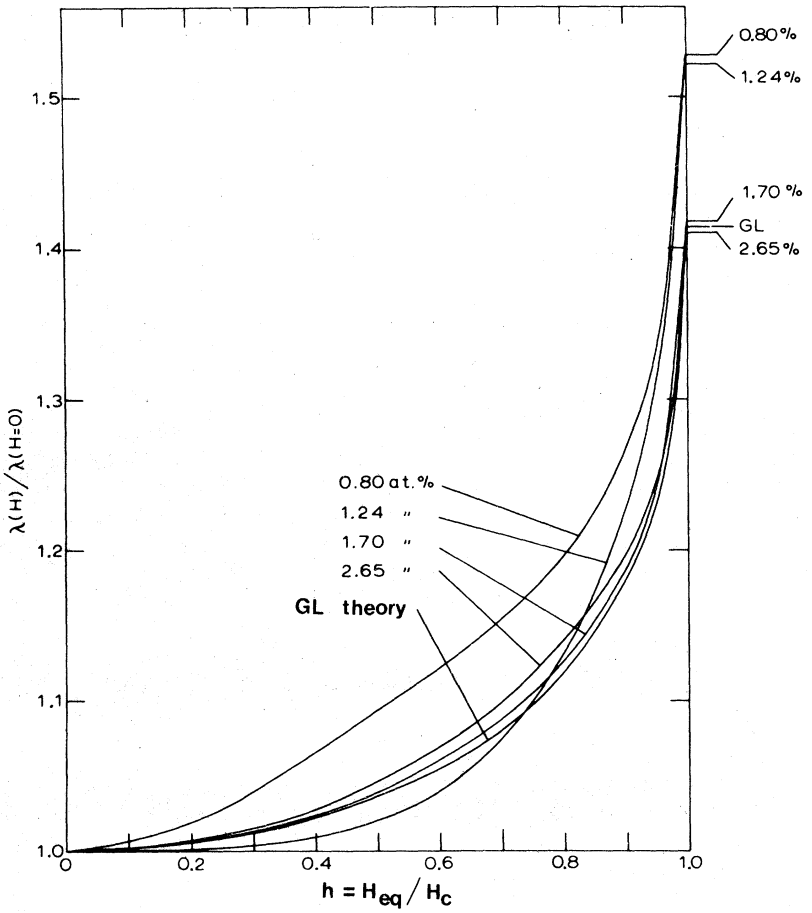

FIG. 9. Final field dependence of the penetration depth λ, for all concentrations. Computed from curves like that of Fig. 8 by empirical inversion of Eq. (4). The extrapolated values at $H = H_{sh}(h = 1)$ are given. The two dirtiest alloys are seen to fit the low-κ GL prediction best. Differences at low h may be due to systematic measuring errors (see text). In conclusion, $\lambda(H/H_{sh})$ comes rather close to being a universal function of H/H_{sh}, independent of κ.

TABLE IV. Experimental results—GL parameter.

at.% Bi	0.80	1.24	1.70	2.15	2.65
κ (Gorkov-Goodman)	0.390	0.585	0.791	1.008	1.216
$\kappa_{c_3}(t=1)$	0.454	0.636	0.835	0.984	1.218
$\kappa_{c_2}(t=1)$	...	...	0.877	1.010	1.251
$\frac{1}{\kappa_{c_3}}\frac{d\kappa_{c3}}{dt}\Big\|_{t=1}$	−0.21	−0.26	−0.40	−0.22	−0.32
$\frac{1}{\kappa_{c_2}}\frac{d\kappa_{c2}}{dt}\Big\|_{t=1}$	...	..	−0.17	−0.33	−0.23
$\frac{d}{dt}\left(\frac{H_{c_3}(t)}{H_{c_2}(t)}\right)_{t+1}$	...	...	−0.37	+0.17	−0.14

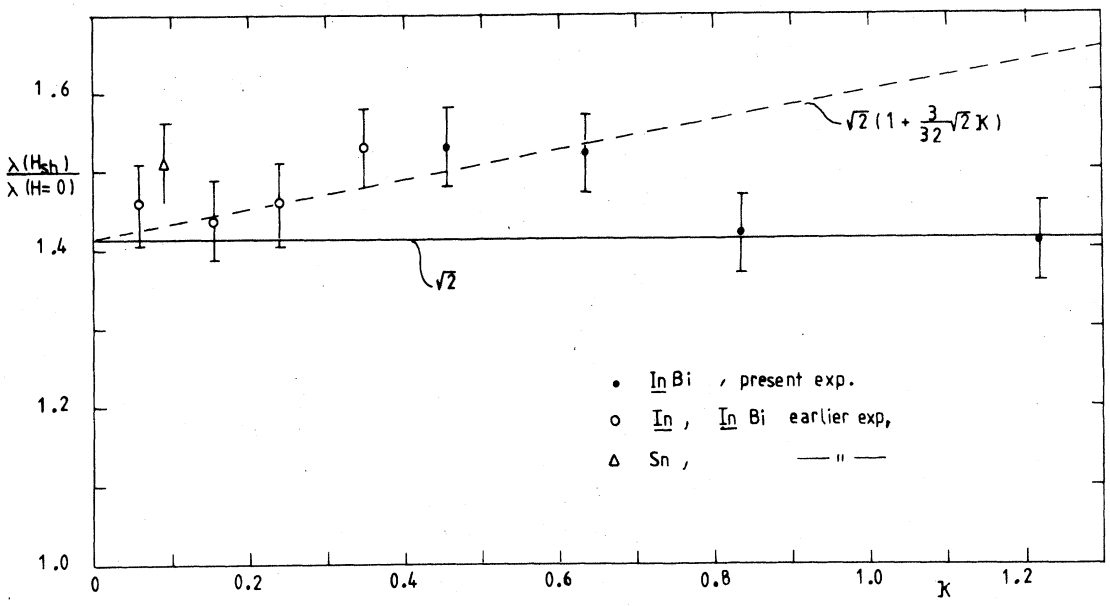

FIG. 10. $\lambda(H_{sh})/\lambda(H=0)$ for all metals investigated to date. Data are consistent with the constant value of $2^{1/2} \cong 1.41$, see solid line. Prediction of Eq. (9), see broken line, is well outside of experimental uncertainties for the higher κ values.

This behavior can be explained in terms of the decrease in mean-free-path l with composition. The derivation of Eq. (18) assumes $l \ll \zeta_0$, the intrinsic coherence length of the pure host metal. For In, we have $\zeta_0 \approx 0.43$ μm. From Table I, we see that we have $l = 0.43$ μm at 0.2 at.%, 0.1 μm at 0.8 at.% and 0.04 μm at 2 at.%. Thus the Gorkov-Goodman relation is accurately verified above $\kappa = 0.9$, where its underlying assumptions are fulfilled, but is surprisingly accurate even at the lower concentration where we have $l \approx \zeta_0$.

D. Superheating field H_{sh}

Besides the measurement of the field dependence of the penetration depth, the determination of the ideal bulk superheating field H_{sh} as a function of κ is the other main objective of the *In*Bi experiments. In previous single-sphere experiments,[1-6] H_{sh} was always larger than H_{c3}, so the sphere would go directly into the normal state, giving a very sharp, large transition. Except for the 0.80-at.% samples, κ is so high in the present experiments that the transition at H_{sh} leads into the intermediate or mixed states. In parallel fields, the superheating transition is then hard to distinguish just by looking at the recorder trace of a complete field sweep. However, it can be unambiguously determined by doing "minor hysteresis loops", slowly increasing the upper field. Then no hysteresis is observed until the upper field reaches H_{sh}, and the Meissner state is destroyed. Also, the superheating transition is much more easily seen in perpendicular fields, and this was used as a check. The bulk of the measurements were in parallel fields. We believe the present measurements to be as accurate as for the low-κ case, although they were more time consuming.

TABLE V. Superheating fields at $t = 1$.

*In*Bi at.%	0.80	1.24	1.70	2.15	2.65
$\kappa_{c_3}(t=1)$	0.454	0.636	0.835	0.984	1.218
$(H_{sh}/H_c\|_{t=1}$	1.78 ±0.05	1.48 ±0.04	1.28 ±0.06	1.17 ±0.09	1.13 ±0.06

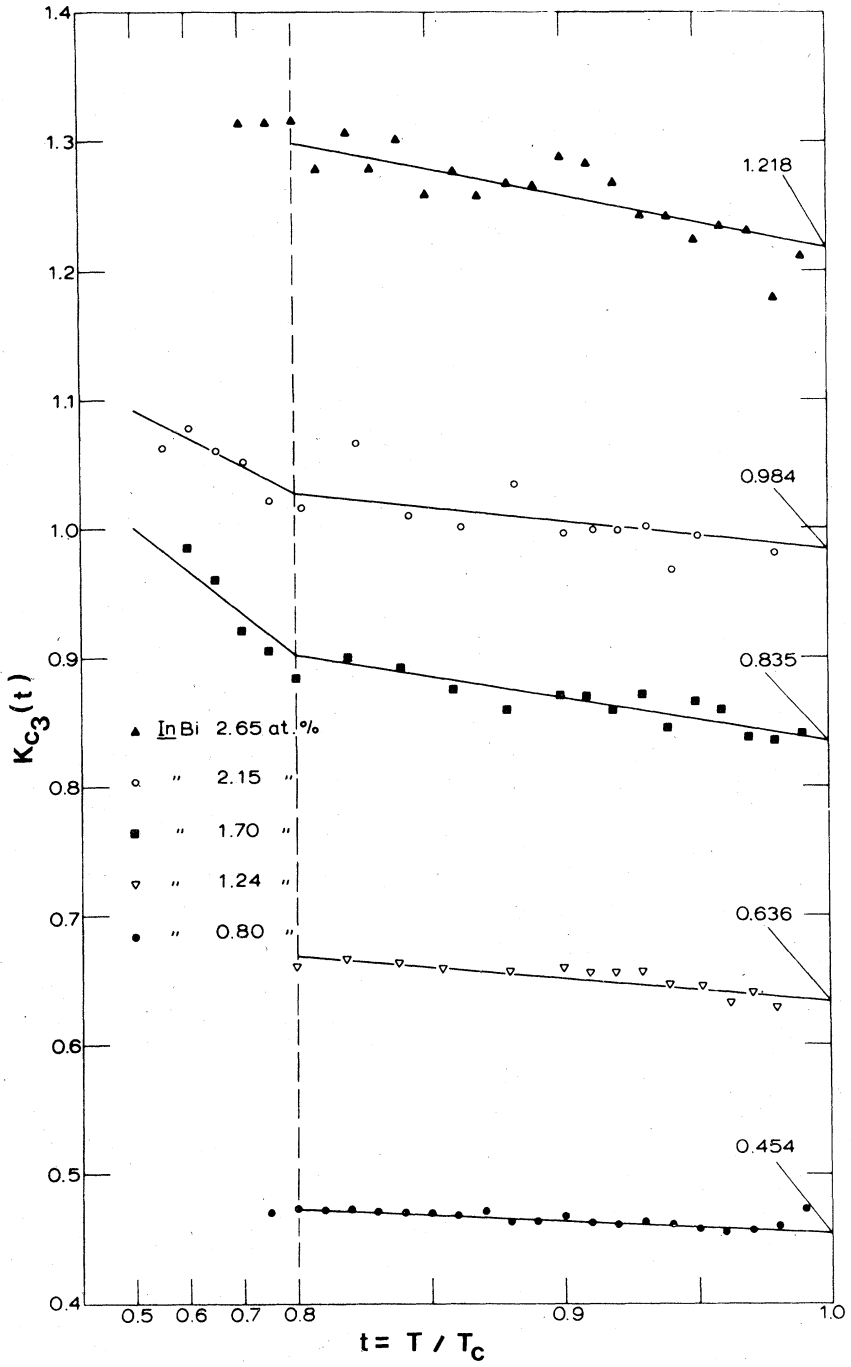

FIG. 11. κ_{c3} as a function of temperature. The extrapolation of κ_{c3} to $t=1$ gives the most reliable value of the Ginzburg-Landau parameter κ.

Figure 13 shows H_{sh}/H_c versus reduced temperature. For four of the concentrations, 0.80, 1.24, 1.70, and 2.65 at.%, the slight temperature dependence leads us to believe that these spheres exhibit ideal superheating above $t=0.8$, and possible for lower t also. Extrapolation to $t=1$ for these samples is straightforward. The 2.15 at.% sample shows abnormally low superheating below $t=0.95$, where the superheating suddenly starts to increase. As experienced previously in β - Ga,[2] this behavior character-

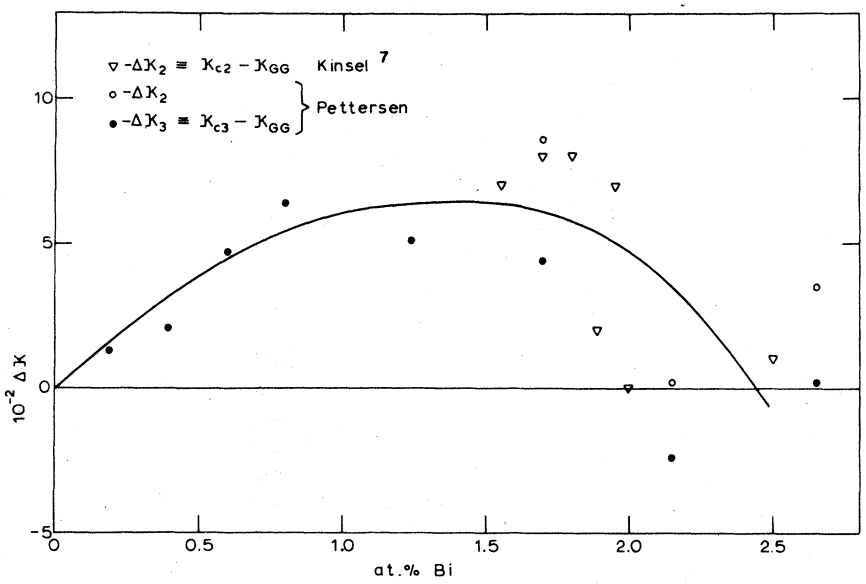

FIG. 12. Deviations of measured values of κ from those computed from the restivity through the Gorkov-Goodman relation, Eq. (18). Note the tendency towards better agreement as impurity content increases, and the assumptions underlying the GG relation become valid.

izes nonperfect samples where defects lead to heterogeneous nucleation of the normal state until the temperature-dependent coherence length $\zeta(t)$ has become so large that it starts neutralizing the effect of the defects. The extrapolation to $t=1$ for this sample is therefore more uncertain. The uncertainty in H_c is still the dominating one, both for the good samples and the bad one. The extrapolated values

TABLE VI. Self-consistent values of κ from H_{c_3} and H_{sh}.

Metal	$\kappa_{c_3}(t=1)$	$D(\kappa^*)$	$\kappa^*(t=1)$	Reference
β Ga	0.141	1.091	0.146 ± 0.003	2,3
Sn	0.0923	1.062	0.097 ± 0.001	4
In	0.061	1.041	0.063 ± 0.003	6
*In*Bi				
0.19%	0.155	1.095	0.151 ± 0.002	6
0.395%	0.240	1.141	0.231 ± 0.003	6
0.60%	0.349	1.204	0.330 ± 0.005	6
0.80%	0.454	1.238	0.410 ± 0.006	Present work
1.24%	0.636	1.336	0.614 ± 0.010	"
1.70%	0.835	1.445	0.852 ± 0.015	"
2.15%	0.984	1.535	1.056 ± 0.035	"
2.65%	1.218	1.664	1.319[a] ± 0.020	"

[a]The error here may be somewhat larger, because we have extrapolated the one-dimensional Gl results beyond $\kappa=1.1$, where they are no longer valid.

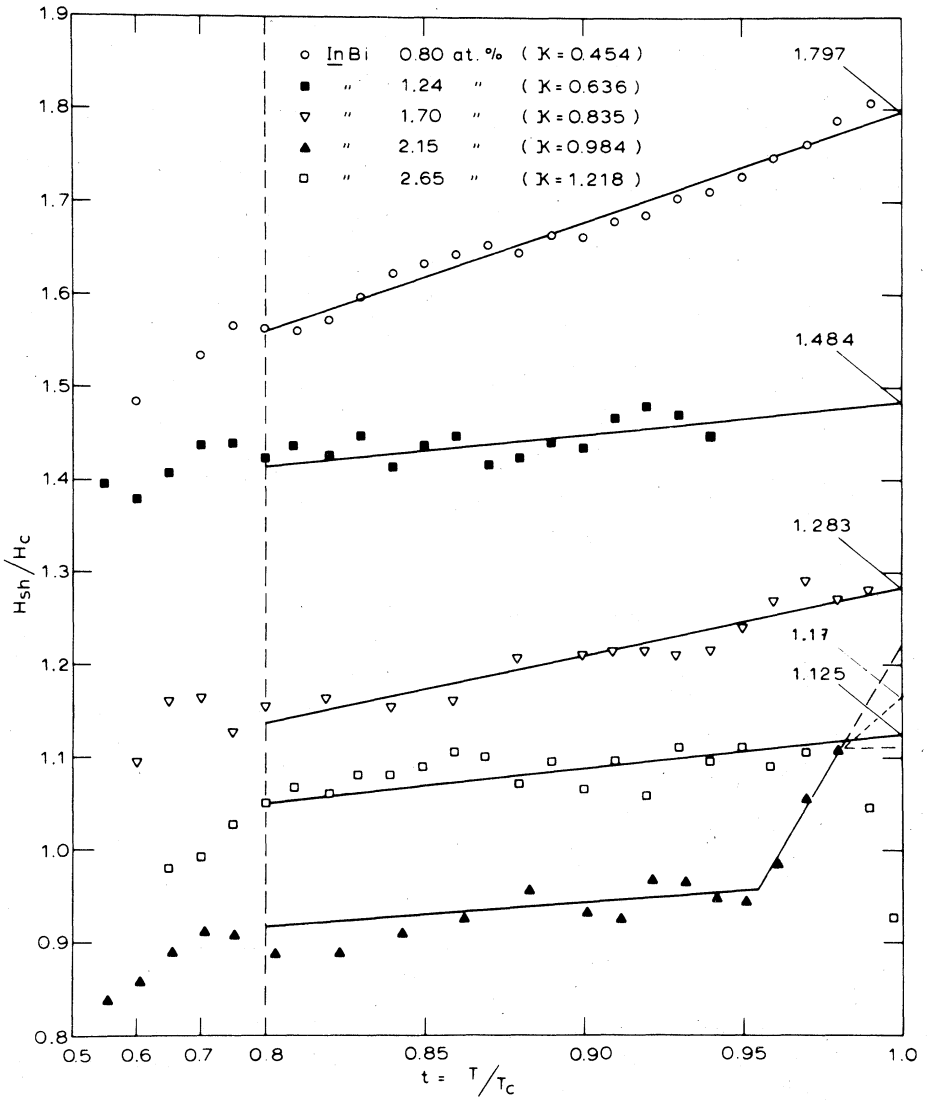

FIG. 13. Superheating field H_{sh} normalized by H_c. Values at $t=1$ are found by extrapolation. All samples are believed to exhibit ideal superheating except the 2.15 at.%. This sample shows abnormally low superheating up to $t=0.95$, where a sudden increase starts. This indicates that defects prevent ideal superheating at low temperatures, but that the defects are neutralized close to t_c because of the increasing coherence length.

are given in Table V.

These values have been plotted with the previous *In*Bi results in the phase diagram of Fig. 1. It is seen that they roughly follow the numerical theoretical predictions of one-dimensional GL theory.[12–14] To look at the details, we can take away the low-κ divergence by multiplying H_{sh}/H_c by $[\kappa(2)^{1/2}]^{1/2}$, and plot the result as a function of κ. This is done in Fig. 14, together with the second-order analytical expression for H_{sh} [Eq. (12)] and the numerical results.[12–14] Almost all the uncertainty is due to that in H_c, which enters both in κ and H_{sh}/H_c. The "knee" at $\kappa=0.45$ is probably related to the corresponding kink in the empirical curve for H_0, (see Fig. 4). With a better knowledge of $H_c(t)$ as a function of *In*Bi composition, these features would quite probably disappear. In conclusion, we believe our measurements to be in good agreement with the numerically calculated H_{sh} in both the type-I and type-II domain, up to $\kappa=1.2$.

E. Self-consistent calculation of κ

Having concluded that the experimental H_{sh} is indeed given by one-dimensional GL theory, let us

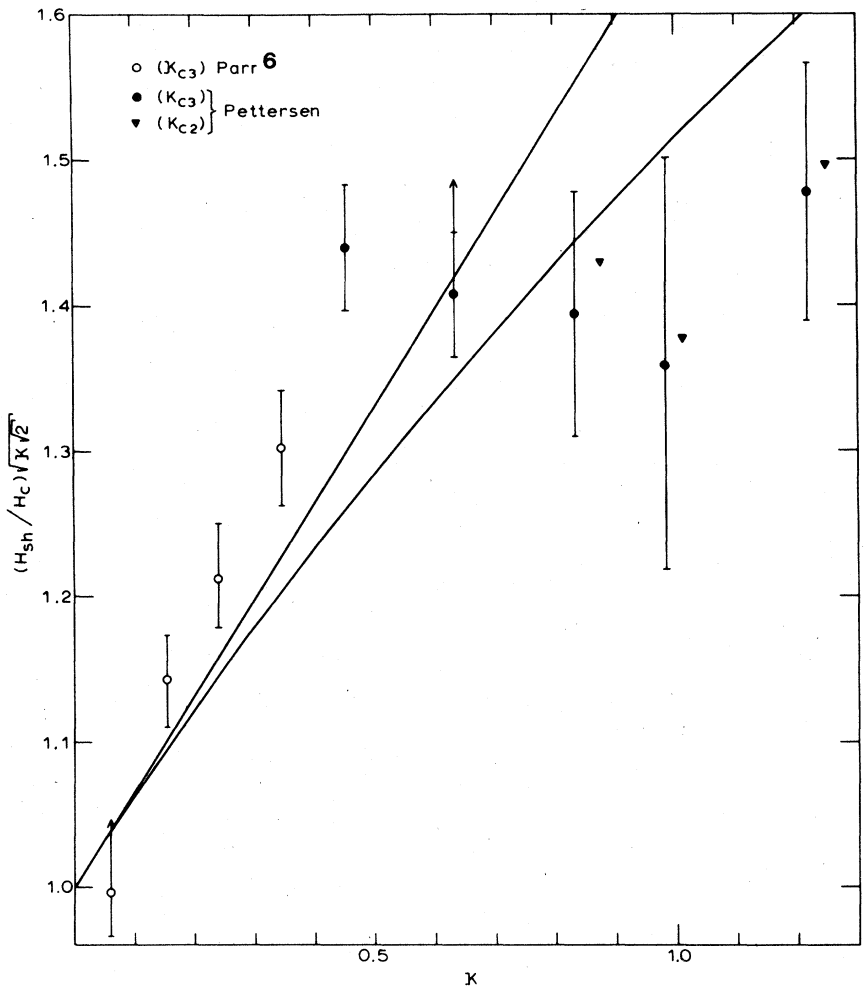

FIG. 14. Deviations in H_{sh}/H_c from the low-κ asymptotic result. Straight line is Parr's second-order analytic expression Eq. (9). Curved line is based on numerical results (Refs. 12–14). The kink at $\kappa \approx 0.5$ may be due to inaccurate choice of H_c, see text. In conclusion, these results verify the numerical calculations of H_{sh}.

now turn the argument around. Assuming the numerical calculation of H_{sh} to be correct, we can use the measured values of H_{c3} and H_{sh} to determine a self-consistent value κ^* of the Ginzburg-Landau parameter at $t=1$. This will be considerably more accurate than either κ_{c2} or κ_{c3}, since knowledge of H_c is not needed. In Table VI, we have done this for all of our past and present single-sphere experiments. The procedure is as follows: we have

$$H_{sh}/H_c = D(\kappa)[\kappa(2)^{1/2}]^{-1/2} \ .$$

First, set $\kappa = \kappa_{c3}(t=1)$, and compute $D(\kappa)$ from the analytical[11] and/or numerical[12–14] calculations, shown in Fig. 14. On combining the defining Eqs. (11) and (12), we then get

$$\kappa^*(t=1) = 2^{-1/6}\left[\frac{\kappa_{c3}(t=1)D(\kappa)}{(H_{sh}/H_c)_{t=1}}\right]^{2/3} , \qquad (19)$$

which is seen to be independent of H_c. If κ^* differs too much from the initial κ_{c3}, a new $D(\kappa)$ is computed, and so on until κ^* is obtained to the desired accuracy. In fact, only one iteration is necessary within the experimental uncertainties, which have been carefully deduced from the data for each metal.

We believe that κ^* may be the most accurate and consistent value of the GL parameter in these metals available by any method to date.

F. Intermediate and mixed states

The rich structure observed in the signal in the intermediate and mixed states (IS and MS) contains information, but it is hard to unravel it. This is so because of an adequate thermodynamic theory for the intermediate state in small ellipsoids is lacking,[6] be-

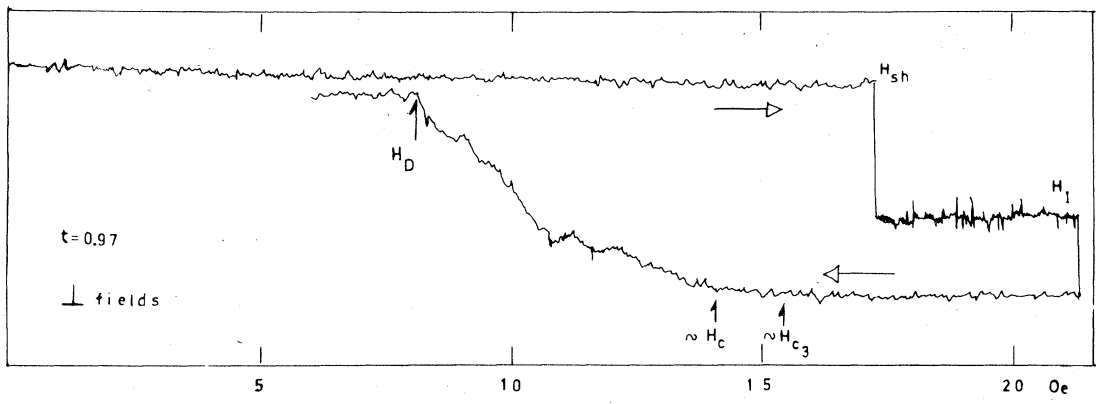

FIG. 15. Recorder trace of field sweep for the *In*Bi 0.80-at.% sphere. After leaving the Meissner state at H_{sh}, the sphere does *not* go normal although the external field is well above H_c. Therefore, a flux bundle must be frozen in along the polar axis, while the equatorial region continues to superheat up to H_I, where the sphere finally goes completely normal. (H_D, demagnetizing field.)

cause of the irreproducibility due to defects, and because of the sensitivity to sweep rates and sweep history. We will therefore just mention a few phenomena from the plethora of observations.[20]

We previously observed[6] in *In*Bi 0.6 at.% ($\kappa = 0.349$) that the IS could be made to superheat far beyond H_c by reincreasing the field once the IS had been reached. We interpreted this as superheating of a superconducting equatorial region around the sphere, while a bundle of flux containing of the order of 100 flux quanta was frozen in along the polar axis.[6] This process is of course helped by the demagnetizing field, since the field at the boundary of the normal and superconducting regions is smaller than the equatorial field. We observe the same phenomenon in the 0.80-at.% sample ($\kappa = 0.45$), with one additional feature: superheating of the IS can now be obtained directly from the Meissner state by increasing the field monotonously from $H = 0$. Figure 15 shows a sample sweep, taken with perpendicu-

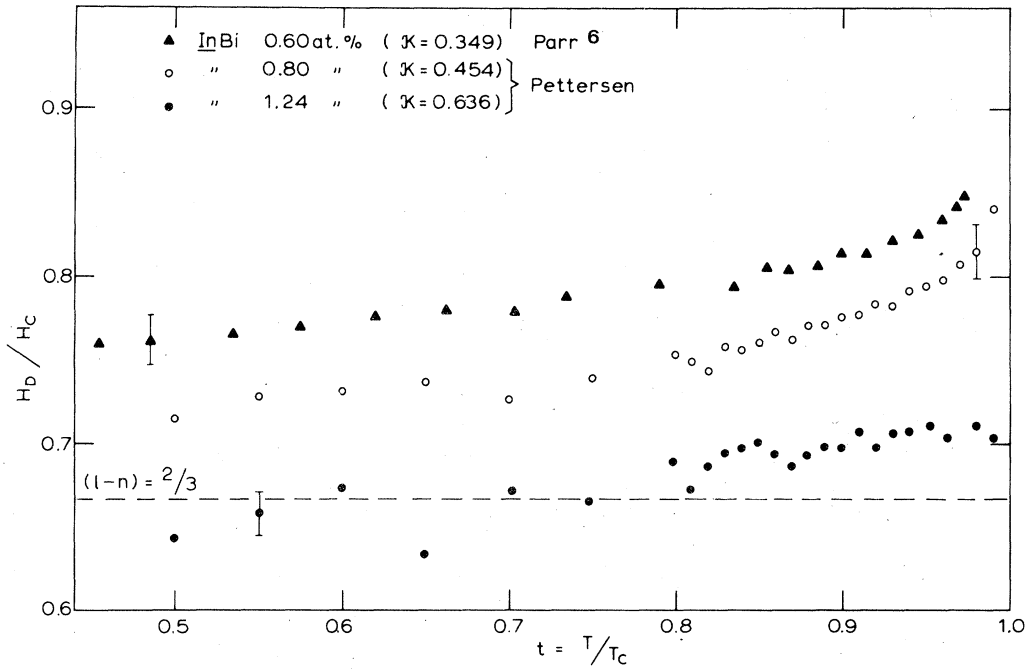

FIG. 16. Temperature dependence of the demagnetizing field H_D normalized to H_c. Deviation from the bulk value of $\frac{2}{3}$ disappears as $\kappa \to 1/2^{1/2}$, where the NS wall surface energy is zero.

lar fields. The Meissner state superheats to the ideal superheating field H_{sh}, well above both H_c and H_{c3}. (These fields cannot be identified in sweep shown, but they were reliably determined in a corresponding sweep in parallel fields at the same temperature). The transition at H_{sh}, however, is seen to lead not into the normal state, but into an IS state, probably of the type suggested above. The transition to the normal state occurs at a still higher field H_{sh}^{I}. At lower temperatures, more such "steps" developed beyond H_{sh}, up to six successive steps were seen in perpendicular fields at $t=0.86$.

The demagnetizing field H_D carries information on the size effect in the thermodynamic equilibrium between the Meissner and intermediate states. For a large sphere, $H_D/H_c=\frac{2}{3}$ independent of temperature. In a small sphere, H_D increases, the increase being governed by the ratio of the surface energy parameter Δ (Ref. 21) to the sphere radius R. Figure 16 shows H_D/H_c for the 0.80 and 1.24% sample, as well as the previous data[6] from 0.60 at.%. As κ increases and Δ decreases, the size effect is seen to be reduced. Since $\Delta\equiv 0$ for $\kappa=1/2^{1/2}$, it is eminently reasonable that H_D/H_c approaches $\frac{2}{3}$ at low t for $\kappa=0.64$.

In Fig. 17, we have combined all these measurements for the three different concentrations. We plot here H_D/H_c vs $\Delta(t)/R$. We have assumed

$$\Delta(t)\cong c\lambda(t)\cong c\lambda_0/(1-t^4)^{1/2}\ .$$

We have estimated $c=\Delta/\lambda$ from Ginzburg's numerical calculations[21] of the surface energy parameter Δ. This gives $c=1.75$, 0.92, and 0.18 for $\kappa=0.349$, 0.454, and 0.636, respectively. Within the experimental uncertainties, the data seem to fall on a universal curve as a function of $\Delta(t)/R$. This may, however, not hold true at low temperatures. The data points for the 0.60-at.% concentration seem to deviate slightly downward from the universal curve for $\Delta/R<1.6$, corresponding to $t<0.75$. This may just indicate that the assumption $\Delta\approx c\lambda_0\gamma$ fails at low temperatures. The same is probably true for the two other concentrations, but it is harder to see it because the uncertainties in the data are larger.

Although there is no theoretical prediction for this size effect in H_D/H_c, the two leading terms should probably be of the form $c_1(\Delta/R)^{\beta}+c_2(\Delta/R)^{2\beta}\cdots$, where we have $\beta=0.4$ or 0.5, and $c_1>0$, $c_2<0$. This insight comes from theoretical results in the

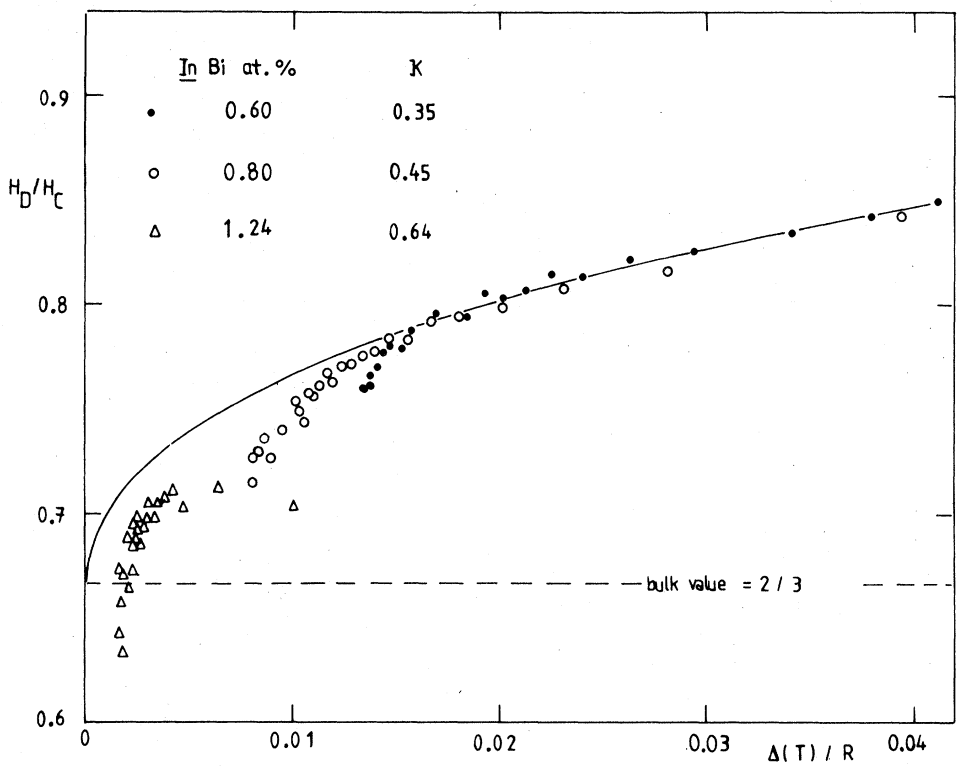

FIG. 17. Data of Fig. 16 plotted as a function of $\Delta(t)/R$, where we have assumed $\Delta(t)\cong c(\kappa)\lambda_0\gamma$, (see text). Within the experimental uncertainty, the data fall on a universal curve. Solid curve is an empirical fit, [Eq. (20)].

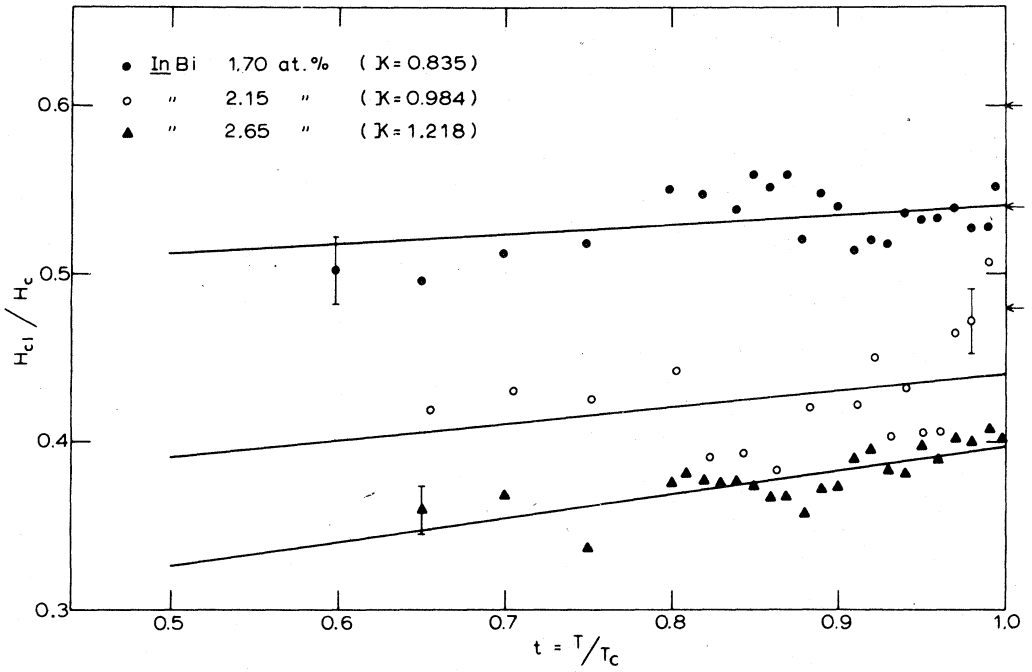

FIG. 18. H_{c1}/H_c for our type-II samples. Numerical values of $(\frac{2}{3})h_{c1}$ are given by arrows. Linear extrapolations lie well below these values, indicating the possibility of supercooling or size effects.

flat-plate geometry.[22,23] In Fig. 17 we have plotted an empirical fit given by

$$H_D/H_c = \tfrac{2}{3} + 1.1(\Delta/R)^{1/2} - 1.0(\Delta/R) \quad . \qquad (20)$$

This is seen to give a fair fit, except for the lower values of Δ/R. Any further analysis of such data must await a quantitative theoretical prediction.

In Fig. 18, we have similarly plotted $h_{c1} = H_{c1}/H_c$ versus temperature for our type-II samples. The values of h_{c1} at $t = 1$ turn out to be 10–20% lower than expected from numerical calculations of h_{c1}.[24] This may be due to supercooling at h_{c1}, or it may indicate a size effect. Similar results were found in observations on *In*Bi 1.84-at.% microcylinders.[25]

V. CONCLUSION

This paper marks the temporary end of a ten year old line of research which started with the pioneering work of Feder and McLachlan.[2] They devised the simple and sensitive mutual-inductance technique for measuring the normal-to-superconducting transition in single spheres, from 5 to 50 μm in diameter. Their work on Sn and In unambiguously established that low-κ metals would superheat all the way to the asymptotic limit given by Ginzburg-Landau theory: $H_{sh} \cong H_c[\kappa(2)^{1/2}]^{-1/2}$. This large superheating cannot be obtained in macroscopic samples, because of nucleation of the normal state by defects. But it is readily attained in small, single spheres individually selected under the microscope for their quality. Feder and McLachlan also studied gold-plated In spheres, thereby verifying experimentally that the ideal supercooling limit for a sphere coated with a normal metal is H_{c2}, while it is H_{c3} for an uncoated sphere.

In their subsequent work on metastable β-Ga, Parr and Feder[2,3] discovered that the magnitude of the superconductive-to-normal transition "jump" varied systematically with temperature, shrinking as T_c was approached. This was successfully linked to the penetration depth $\lambda(t)$, and led to the much more precise and controlled experiments by Parr on Sn,[4] and the low-κ *In*Bi alloys.[5,6] Both the temperature and field dependence of λ were measured in this way. Until then, no measurements of $\lambda(H)$ existed above H_c, for the simple reason that the macroscopic samples used did not superheat. The experiments on Sn (Ref. 4) were the first to measure $\lambda(H)$ all the way to the ideal superheating limit. They showed a strong increase in λ close to H_{sh}. Ginzburg-Landau theory predicted $\lambda(H_{sh})/\lambda(0) = 2^{1/2}$. The value found in Sn was 1.51 ± 0.04, the subsequent experiments on *In*Bi came even closer to the predicted value, (Ref. 5 and this work). In the present paper, the *In*Bi experiments are extended from the type-I domain well into the type-II domain, up to $\kappa \sim 1.2$. We are observing ideal superheating in both domains, and the experi-

mental results are in good agreement with the numerical calculations based on GL theory. Indeed, H_{sh} is the stability limit of the Meissner state, and is not influenced in any way by the transition from type-I to type-II superconductivity, except in that the final state *after* the transition has occured, is the mixed rather than the intermediate state. The same is true for the field dependence of the penetration depth. This work shows that $\lambda(H)/\lambda(H=0)$ is very close to being a universal function of H/H_{sh}, independent of κ, and irrespective of type-I or type-II superconductivity.

The subject of reversible and irreversible transitions in intermediate-size superconductors has became a very mature subfield of superconductivity research. It is fitting that a comprehensive review paper was dedicated to it recently.[26] In our opinion, time has now come to alter the detection system for the single-sphere method so as to increase the signal-to-noise ratio by at least one order of magnitude. SQUID (superconducting quantum-interference device) detection should be studied, possibly together with thin-film sampleholders. This would make possible the study of spheres around 1 μm in diameter or even smaller. A host of size effects and metastability problems could then be explored in much greater detail. Meanwhile, it is interesting to note that a technique has recently been found to study the superheating field in nonperfect, macroscopic samples. Yogi[16] recently showed that samples subjected to rf fields at 90–300 MHz stayed in the Meissner state until the amplitude exceeded H_{sh}. In dc fields, the same samples showed almost no superheating. This shows that the defects which cause heterogeneous nucleation of the normal state at dc (and also at 75 kHz, which is the tickling field in our experiments) are rendered inoperative as nucleation centers at rf frequencies. This may have important consequences for fusion applications. It establishes rf experiments as a supplement to the single-sphere technique for studying superheating.

ACKNOWLEDGMENTS

We are grateful to A. Skjeltorp and T. H. Wettre for assistance in reducing the data, and to B. Berling and H. Bratsberg for technical assistance.

---

†Present address: Ministry of Oil and Energy, Oslo-Dep, Norway

*Based on thesis in partial fulfillment of the requirement for the cand. real. degree.

[1]J. Feder and D. S. McLachlan, Phys. Rev. 177, 763 (1969).
[2]H. Parr and J. Feder, Phys. Rev. B 7, 166 (1973). (Partly superseded by Ref. 3).
[3]H. Parr, Phys. Rev. B 10, 4572 (1974).
[4]H. Parr, Phys. Rev. B 12, 4886 (1975).
[5]H. Parr, Phys. Rev. B 14, 2842 (1976).
[6]H. Parr, Phys. Rev. B 14, 2849 (1976).
[7]T. Kinsel, E. A. Lynton, and B. Serin, Rev. Mod. Phys. 36, 105 (1964).
[8]C. Valette and J. P. Burger, J. Phys. (Paris) 30, 562 (1969).
[9]The Orsay Group, in *Quantum Fluids,* edited by D. F. Brewer (North-Holland, Amsterdam, 1966), p. 26.
[10]R. Esfandiari and H. J. Fink (private communication).
[11]H. Parr, Z. Phys. B 25, 359 (1976).
[12]J. Matricon and D. St-James, Phys. Lett. A 24, 241 (1967).
[13]H. J. Fink and A. G. Presson, Phys. Rev. 182, 498 (1969).
[14]R. S. Poulsen and H. J. Fink (private communication).
[15]K. Førsvoll and I. Holwech, Phil. Mag. 10, 181 (1964).
[16]T. Yogi, Ph.D. thesis, (Caltech, 1976) (unpublished); T. Yogi, G. J. Dick, and J. E. Mercereau, Phys. Rev. Lett. 39, 826 (1977).
[17]D. U. Gubser, D. E. Mapother, and D. L. Connelly, Phys. Rev. B 2, 2547 (1970).
[18]R. C. Carriker and C. A. Reynolds, Phys. Rev. B 2, 3991 (1970).
[19]B. B. Goodman, IBM J. Res. Dev. 6, 63 (1962).
[20]G. Pettersen, thesis for the cand. real. degree, (1978) (unpublished). In the thesis, the intermediate and mixed states are treated in more detail, as well as observations of supercooling of the bulk of the sphere while the surface was superconducting. This occurred in the 1.24-at.% sphere, corresponding to $\kappa=0.64$. This sphere showed 4–5% hysteresis around H_c, for $t<0.8$, while the surface superconductivity remained up to $H_{c3}\approx 1.5H_c$.
[21]See for example V. L. Ginzburg, Physica (Utrecht) 24, S42 (1958).
[22]L. Landau, J. Phys. (Moscow) 7, 99 (1943).
[23]M. Tinkham, *Introduction to Superconductivity* (McGraw-Hill, New York, 1975), p. 95.
[24]J. L. Harden and V. Arp, Cryogenics 3, 105 (1963).
[25]D. S. McLachlan, Solid State Commun. 8, 1595 (1970).
[26]H. J. Fink, D. S. McLachlan, and B. Rothberg-Bibby, in *Progress in low-temperature physics,* edited by D. F. Brewer (North-Holland, Amsterdam, 1978). Vol. 7b, Chap. VI, p. 431.